

A simple atomistic model for the simulation of the gel phase of lipid bilayers

G. La Penna^{a)} S. Letardi^{b)} V. Minicozzi^{c)}
S. Morante^{c)d)*} G.C. Rossi^{c)e)} G. Salina^{e)}

^{a)}Istituto di Studi Chimico-Fisici di Macromolecole Sintetiche e Naturali, CNR
Via De Marini 6, 16149 Genova, Italy

^{b)}ENEA, Casaccia

^{c)}Dipartimento di Fisica, Università di Roma *Tor Vergata*

^{d)}INFM, Unità di Roma 2

^{e)}INFN, Sezione di Roma 2

Via della Ricerca Scientifica, 00133 Roma, Italy

November 12, 2018

^{*)}*Correspondence to:* Silvia Morante, Dipartimento di Fisica, Università degli Studi di Roma “*Tor Vergata*”, Via della Ricerca Scientifica, 00133 Roma, Italy (Phone Number: +39-0672594554; FAX Number: +39-062025259; E-mail address: morante@roma2.infn.it)

Abstract

In this paper we present the results of a large-scale numerical investigation of structural properties of a model of cell membrane, simulated as a bilayer of flexible molecules in vacuum. The study was performed by carrying out extensive Molecular Dynamics simulations, in the (NVE) *micro-canonical ensemble*, of two systems of different sizes (2×32 and 2×256 molecules), over a fairly large set of temperatures and densities, using parallel platforms and more standard serial computers. Depending on the dimension of the system, the dynamics was followed for physical times that go from few hundred of picoseconds for the largest system to 5–10 nanoseconds for the smallest one. We find that the bilayer remains stable even in the absence of water and neglecting Coulomb interactions in the whole range of temperatures and densities we have investigated. The extension of the region of physical parameters that we have explored has allowed us to study significant points in the phase diagram of the bilayer and to expose marked structural changes as density and temperature are varied, which are interpreted as the system passing from a crystal to a gel phase.

1 Introduction

The simulation of realistic models of cell membranes is of the utmost importance, if not for immediate medical use, certainly for the development of new conceptual and practical tools in the application of Molecular Dynamics (MD) methods to these and similarly complex systems. A lot of research activity has gone in this direction (see for instance [1, 2, 3, 4, 5, 6] and references therein), but we are still far from having a complete understanding of the dynamic and thermodynamic properties of this kind of systems, not to mention the problem of simulating the formation and the dynamics of pores and ion channels (see, however, the recent very interesting work of ref. [7]).

To predict the structure of molecular layers in different physico-chemical conditions by computer simulations, several modeling strategies have been proposed and investigated. Among them we would like to mention the following.

1) Atomistic detailed approaches in which bilayer constituent molecules, water and possible counter-ions are modeled explicitly in full detail. The interaction between electrostatic point charges are evaluated through Ewald related summation techniques, while the bias due to the use of periodic boundary conditions is reduced by performing simulations in extended *ensembles*. Recent examples of this

kind of investigations can be found in refs. [3, 4, 8].

2) Simplified models of structures formed by surfactants have been constructed that retain some of the essential interactions between the constituent particles, like the Lennard-Jones (LJ) forces among the hydrophobic tails and between solvent and hydrophilic molecular heads. On top of them an *ad hoc* repulsive soft core describing the interaction between hydrophobic and hydrophilic particles is added to allow self-assembling of micelles and bilayers [9].

3) Models in which only a single molecule or chain is modeled explicitly in terms of a realistic all-atom description, while the effect of the remainder of the system is parametrized by a mean-field deterministic force plus appropriate random forces. Models of this type are successfully treated by Monte Carlo simulations and/or stochastic techniques. In this context we wish to recall the fairly good agreement with experiments obtained in the evaluation of the NMR deuterium order parameters in the case of lipid bilayers, when Brownian Dynamics is used for their simulations [10].

4) In the field of liquid crystals, where certain properties of layers often can be explored only through computer simulations, even more simplified force-fields, like that proposed by Gay and Berne [11] (GB hereafter) with the successive modifications of refs. [12] and [13], are used. Despite their simplicity these models allow the exploration and the study of various phases of the system, including smectic phases characterized by a number of different tilt angles.

Comparing different models and trying to assess the effects of the various contributions that are included or neglected in different instances, is not a simple task. An example of this situation is the comparison between the GB potential [11] and its closest LJ representation. The GB potential was originally devised so as to mimic the interaction between two identical linear arrays composed by four LJ sites each. The properties of a fluid made of GB particles turn out to be rather different from its LJ counterpart: the GB fluid has a phase diagram with a well characterized nematic-isotropic transition temperature, while apparently the LJ counterpart does not show any phase transition of this kind when only the temperature is varied. This is a case where the use of a simplified potential, far from leading to an impoverishment of the model, turns out to give rise to an unexpected and very interesting thermodynamic behaviour.

In the case of lipid molecules the comparison among different modeling strategies are much more difficult because of the occurrence of different types of interaction sites (head, tail and solvent) and because of the special importance of the internal molecular degrees of freedom, that may greatly influence the inter-molecular interactions, as well as the related hydrophobic tail packing and bilayer stability properties.

The purpose of this paper is to perform MD simulations of a simplified, but still

sufficiently rich model of molecular bilayer in vacuum. The bilayer constituents are branched molecules composed by LJ sites with the topology and the internal flexibility of the two fatty acid tails and glycerol group of the *Dimyristoyl-phosphatidylcholine* (DMPC hereafter) molecule. In the absence of water, the charged part of the DMPC head has been replaced by a methyl group (see Fig. 1).

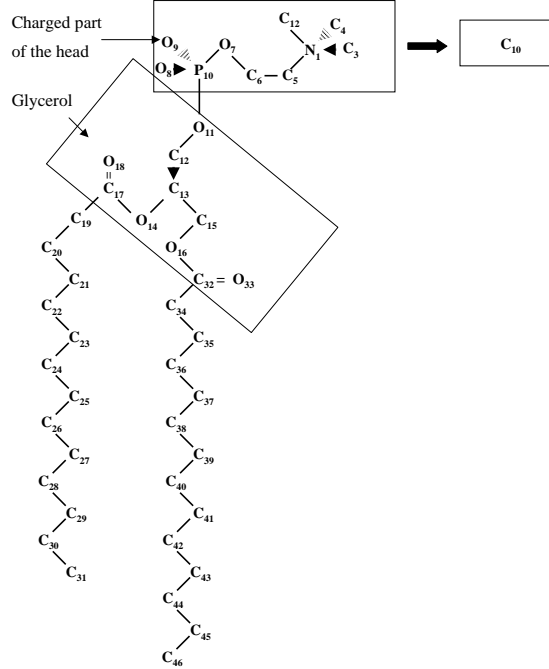


Figure 1: The chemical structure of the DMPC molecule and the substitution which transforms it into what we have called DMMG. Hydrogens are not drawn. Carbons in the CH_n groups are labeled progressively in the standard way.

With respect to an all-atom description of DMPC bilayers [6], we retain in the model only the LJ interactions between the most hydrophobic portions of the lipid molecules together their intra-molecular flexibility. These simplifications allow us to single out and investigate the role of repulsive-dispersive interactions in

the structure of the bilayer, without the complications arising when electrostatic interactions among heads and solvent are present, which substantially limit the length of the simulated trajectories.

Owing to these circumstances we are able to generate very long trajectories (up to ~ 10 ns) of sufficiently large systems, which allow us not only to expose and control certain effects related to the slow equilibration of the system (which would be important sources of systematic errors in the analysis of simulations not sufficiently longer than 1 ns), but also to accurately check the physical consistency of the parameters of the employed intra-molecular potential.

We notice that in the simplified approach we present in this paper the bilayer components are not really amphiphilic. This is not, however, a completely silly approximation. We have checked, in fact, that the system configurations, occurring at the lowest density we have explored, in which it happens that some of the molecule tails are turned up-side-down, have approximately the same potential energy as the physical situation in which the tails of the molecules of the two layers are in contact. We find instead that at the surface density of both the crystal and gel phases the energy barrier which should be overcome by a molecule to rotate up-side-down by 180° degrees is sufficiently high to prevent this event to occur in the whole range of temperatures we have explored. This observation makes us confident that the predictions we have for the structural properties of the system in these two phases are fully reliable. As we said the situation, is completely different at our lowest density, which corresponds to that of the liquid-crystal phase. Evidently in this case the potential barrier is not sufficiently high, as we witness the crossing of it by some of the molecules. Despite this unphysical feature, we remark that our bilayer model remains stable at all the values of temperature and density we have studied (even at the lowest one), in the sense that, thanks to the strong attractive interactions between the two layers, none of the molecules leaves the layers.

We also notice that at low surface density the potential energy of the whole system is presumably smaller than it would be if the repulsion between solvent and tails were introduced. In models in which solvation effects are included [8, 9] low density configurations are essentially inaccessible, precisely because of a substantial solvent-tail repulsion.

Given the crudeness of our bilayer model, we do not expect to be able to accurately predict thermodynamic parameters, like the dependence of the surface density or the magnitude of the stress tensor [4, 8] as functions of the temperature, mainly because of the lack of the interactions that govern the structure of the solvent interface and the absence of terms in the force-field that would prevent the tendency to isotropization at much too low surface densities we have mentioned above. Therefore, in order to study the physics of the different phases of our bilayer

model, we decided to fix the surface density at the experimentally estimated values (*NVE*-simulations), rather than trying to work in an extended *ensemble* at fixed (lateral) pressure.

As for the role of water, we tentatively assume that, once the bilayer is formed in the polar fluid, its structural and thermodynamic behaviour will be mainly governed by the packing and flexibility properties of the hydrocarbon tails [14]. Most of the effects of water on the detailed physico-chemical behaviour of the membrane are indeed of secondary importance for the kind of questions we are addressing here. In the picture we have in mind, in fact, water is only important in that it behaves as a sticky medium for the lipid heads, which modulates the surface density by more or less penetrating into the bilayer [15]. Thus water penetration is held responsible for the difference one sees in the increase of disorder in the head region, as compared to what happens to the tails, only to the extent it affects the surface density of the bilayer. The different behaviour between heads and tails may in turn be at the origin of the great sensitivity of the structure of the phase diagram to molecular composition and tail length.

Even in the simplified model we are considering here, the known crystal structure of the glycerol group and fatty acid tails of DMPC [16] is well accommodated in a local minimum of the force-field we are using, at the appropriate surface density. The comparison of our results with those of more refined models can be of great help in understanding the relevance of more realistic modelizations of the molecular components of the system and/or the role of water.

The MD simulations we have performed extend over a rather fine grid in the temperature-density plane. Thanks to this resolution and to the large statistics we have collected, we are able to draw interesting conclusions on the role of LJ interactions and internal flexibility on the stability and the structural properties of the crystal and gel phases of our bilayer model.

The paper is organized as follows. In section 2 we describe the model of bilayer we have constructed and investigated. In section 3 we discuss the details of our simulation strategy and in section 4 we report the most significant results we have obtained with a special emphasis on the information we have collected concerning structure and properties of the crystal and gel phases of the system. Conclusions can be found in section 5.

2 Simulation set-up

Schematically, a cell membrane can be described as an almost spherical bilayer consisting of phospho-lipid molecules which separates the interior of the cell from the external world. Phospho-lipids are molecules composed by a hydrophilic head

and one or two hydrophobic tails. These peculiar hydropathicity properties lead to the well known two-sheet structure of the membrane, in which the hydrophilic heads are in contact with water, present both outside and inside the cell, while the hydrophobic tails are more or less tail-to-tail pair-wise aligned.

It appears experimentally that an important parameter governing the reaction rate of many biological processes, taking place inside or in the near vicinity of a membrane, is its “permeability” [14]. From this point of view a membrane can be thought as a system made out of two layers of a smectic fluid, with a permeability which depends “critically” on temperature, density, the detailed chemical composition of the constituent phospho-lipids, the concentration of chemicals possibly dispersed in the membrane itself or in the solvent, etc.

It is clear that a detailed simulation of the dynamics of the membrane of a living cell is just impossible and one has to resort to a number of simplifications. A fortunate circumstance in this respect is that it appears experimentally that the nature and the location of the phase transitions, which control a number of important physico-chemical properties of the membrane, are essentially related to the bulk ordering properties of the hydrophobic tails [14]. Thus a first step in the direction of simulating a realistic system, and the one which has been also largely followed in the literature [1, 2, 4, 6], is to take a two sheet system, each consisting of the largest possible number of lipid molecules (compatibly with the available computer power), in presence or even in absence of water, and proceed to study how the relevant order parameters behave as functions of temperature and surface density and what are the structural properties of the system in the different regions of its phase diagram.

Lacking any realistic theoretical modeling of mesoscopic systems, as membrane or other molecular aggregates of biological relevance, one must resort to numerical methods, like MD or Monte Carlo and stochastic simulations of various kinds, in order to study the dynamic and thermodynamic behaviour of such complex systems.

MD provides us with a microscopic, most often, classical ¹ description of the system, which consists in following its time evolution by solving numerically the Newton equations of motion of its elementary constituents.

The general mathematical setting of MD for the simulation of diffusive systems is well known [18] and we will not dwell on it here. For a general presentation of the method with a discussion of some of the tricks that have been developed to efficiently implement MD codes on the existing most powerful parallel platforms in the case of (*NVE*) simulations, we refer the reader to [19].

We have prepared two chemically identical samples of largely different size

¹Car and Parrinello [17] have proposed a consistent quantum mechanical generalization of the MD approach.

of our bilayer model, consisting of 2×32 and 2×256 molecules, hereafter denoted for short $BM(S)$ and $BM(L)$ (“ S ” and “ L ” stand for “small” and “large”, respectively). Since, as we said in the Introduction, we do not have explicitly water in our simulations, we will neglect electrostatic interactions altogether. For consistency we have taken, as a model for the constituent molecules, an artificial variant of DMPC, christened by us DMMG (*Dimyristoyl-methyl-glycerol*), in which the charged part of the DMPC head (defined as the part of the molecule above the first atom—a P atom—bound to the glycerol oxygen) has been replaced by a single CH_3 group. The detailed chemical structure of the Y-shaped DMPC molecule is shown in Fig. 1, where we have also indicated the modification we have made on its structure in order to construct the artificial variant of it we will be dealing with in this paper. The elementary constituents of the DMMG molecule will be schematically represented by LJ sites centered on the CH_n groups ($n = 1, 2, 3$), thereby using the so-called “united atom” approximation. In this way each DMMG molecule will consist of 37 elementary units (for short simply “atoms” in the following). Intra-molecular and fully flexible inter-molecular interactions are described by making reference to the OPLS force field [20] with the modifications introduced in ref. [21]. According to the general OPLS philosophy, we have reduced the strength of the 1-4 LJ potential in each dihedral angle by a factor 8. The inter-molecular potential was linearly switched off between 1.0 and 1.1 nm. As we already said, no electric charges are attributed to atoms.

We have assumed the crystallographic density of our artificial system, ρ_o , to be the same as that of DMPC [16]. Experimentally the DMPC crystallographic surface density corresponds to an area of 0.396 nm^2 per molecule in the plane of the bilayer (the x - y plane). Despite the fact that we have drastically simplified the structure of the head of the constituent molecules, we decided to keep the same number of molecules per unit area as in the case of a DMPC bilayer, in order to be able to compare the properties of our model with those of a somehow related real system. At crystallographic density the surface of the system $BM(S)$ spans an area of $3.56 \times 3.56 \text{ nm}^2$, that of the system $BM(L)$ an area 8 times larger, equal to $14.24 \times 7.12 \text{ nm}^2$.

The separation of the two layers in the z direction is fixed at the beginning of each simulation by setting the distance between the branching points (the C13 atoms in the picture of Fig. 1) of two opposite molecules, equal to 4.4 nm.

In order to build the initial bilayer configuration we have started by generating a molecule with the dihedral angles of molecule A in Table 1 of ref [16]. Tail #1 of this molecule ² was taken to lie in the z - y plane, parallel to the z axis, with the head pointing in the positive z direction. Notice that tail #1 shows a kink

²To be definite we call tail #1 the shortest of the two DMMG tails (the O14-C31 tail in Fig. 1) and tail #2 the longest one (the C15-C46 tail).

in correspondence to the dihedral angle O14-C17-C19-C20, making it parallel to tail #2 after C19. The basic molecule of the lower layer is generated by performing a rigid rotation of the first molecule by 180° around the y axis, holding fix the C13 atom. The two C13 atoms are then displaced by 4.4 nm, by translating one molecule with respect to the other one along the z axis. The fundamental cell of the initial crystal is an orthorhombic prism with the square basis in the x - y plane and the longer edge along the z axis. Two copies of this pair of molecules have been placed in the cell with the C13 atoms of the lowest molecules located one in a vertex and the other in the center of the x - y face, respectively. Finally the fundamental cell is replicated in the x and y directions the necessary number of times (*i.e.* 4×4 and 16×8 times, respectively).

As usual, to limit finite-size effects, both $BM(S)$ and $BM(L)$ samples are taken to be periodic in the x and y directions. For simplicity of computation, periodicity is also imposed in the z direction, but adjacent copies of the bilayer are separated by about 100 nm, a distance so large that there are no possible interactions among different copies of the system.

Two different MD codes, expressly developed by our group, were employed for the simulations of the two systems. Both codes make use of an MTS integration algorithm [22, 23] with a long time step of 5 fs. A short time step 10 times smaller is introduced to integrate stretching and bending contributions. The package used for the $BM(S)$ system (2×32 molecules) was run on a Digital 500 α -station. The code produces 1 ps of simulated dynamics every $\simeq 100$ s of CPU-time (corresponding to 0.5 s of CPU time for every long time-step for a system of 2368 atoms). For the larger $BM(L)$ system (2×256 molecules) we have employed a parallel version of the previous code. This code evolved from the one we used in [19] to test the level of the performances offered by parallel platforms in MD simulations of diffusive systems. Given the large request of computing power necessary to perform simulations of such a big system, use was made of the parallel platform called *Torre*, the largest (512 nodes, 25 Giga-flops) of the today available APE computers [24]. On this platform producing 1 ps of simulated dynamics costs $\simeq 2000$ s of CPU-time (which corresponds to 2 s of CPU time for every long time-step for a system of 18944 atoms).

In Tables 1 and 2 we report for the two samples ($BM(S)$ and $BM(L)$) we have constructed the set of values of surface density and temperature (T in Kelvin), at which simulations have been carried out. The surface density is expressed in units of the crystallographic density ρ_o through the formula $\rho = \mu \cdot \rho_o$. The numbers in the entries of the Tables represent the length of the corresponding trajectory.

At every density value, the sample $BM(S)$ has been brought at the required temperature by a simple velocity-rescaling algorithm, which was run for more than 100 ps in the worst case. The surface density of the bilayer was fixed at

Table 1: The set of densities ($\rho = \mu \cdot \rho_o$, ρ_o = crystallographic density) and equilibration temperatures (T) at which we have run the simulations of the system $BM(S)$. The numbers in the entries of the Table represent the length of each trajectory in ns, not counting the initial velocity-rescaled steps.

$T(K) // \mu$	1.05	1.0	0.95	0.91	0.87	0.83	0.79	0.76	0.69
150	0.9	5.4	0.9	0.9	0.9	5.4	0.9	0.9	5.4
225	0.9	5.1	0.9	0.9	0.9	0.9	0.9	0.9	0.9
250	0.9	5.1	0.9	0.9	0.9	0.9	0.9	0.9	0.9
275	5.1	5.4	0.9	0.9	0.9	5.4	0.9	0.9	5.4
300	0.9	5.1	0.9	0.9	0.9	0.9	0.9	0.9	0.9
325	0.9	5.4	0.9	0.9	0.9	9.9	9.9	0.9	5.4
350	0.9	5.1	0.9	0.9	0.9	5.4	0.9	0.9	0.9

the chosen value at the beginning of each simulation by uniformly rescaling the x and y coordinates of the center of mass of each molecule by the factor $\sqrt{\mu}$. The initial configuration of the larger system, $BM(L)$, was obtained by replicating the last available configuration of $BM(S)$ with the desired values of temperature and density, and then equilibrating the whole system for further 40 ps, again using a velocity-rescaling algorithm. Throughout this paper we will indicate for short by T the equilibration temperature, *i.e.* the temperature held fixed during the velocity-rescaling steps, and by T_s the real temperature at which the simulation was actually run. Of course the two temperatures will be somewhat different from each other. For most of our considerations in this paper this difference will be of little importance.

Table 2: Same as in Table 1 for the system $BM(L)$. Trajectory lengths are in ps.

$T(K) // \mu$	1.05	1.0	0.95	0.87	0.83	0.79	0.69
150	•	140	•	•	140	•	140
225	40	60	40	40	•	40	•
275	40	140	60	40	140	40	140
300	•	60	•	•	•	•	•
325	40	140	40	40	140	40	140
350	40	60	40	40	•	40	•

Few comments are in order here.

1) The simulations of the small system $BM(S)$ are particularly long (they range from a minimum of 0.9 ns up to a maximum of 9.9 ns, not counting the initial velocity-rescaling equilibration steps) and span a grid of $7 \times 9 = 63$ points in the temperature-density plane (Table 1). Notice that the trajectories employed in the analysis presented in the next sections are all longer than 5 ns.

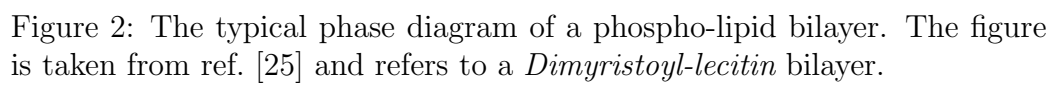
2) $BM(L)$ simulations cover a similarly large region of temperatures and densities with a total of 28 points. Trajectories are, however, much shorter (Table 2).

3 Simulation strategy

One of the reasons to perform Molecular Dynamics simulations of such complex systems, like cell membranes, is that many biological processes are still waiting for an explanation at molecular level. Not many of the experimental techniques presently available may reach this goal at the resolution required and under really well controlled physico-chemical conditions. On the other hand, it is obvious that in order to be reasonably confident about the validity of the model used in a simulation, the structural properties of the model must be carefully compared to those of the “real” system so as to check the quality of the correspondence between simulation results and actual experimental data.

In the case we are investigating, one of the most interesting macroscopic features characterizing the biological behaviour of the system is the structure of its phase diagram. The typical phase diagram of a phospho-lipid bilayer is reproduced in Fig. 2. The figure is taken from ref. [25] and refers to a *Dimyristoyl-lecithin* bilayer. As it is also seen from the figure, many phases have been identified experimentally: the most clearly separated ones are those called L, L_β and L_α , corresponding to the crystal, gel and liquid-crystal phase of the system, respectively. It is important to note here for the future comparison with simulation data that the horizontal axis in Fig. 2 is the percentage of water per phospho-lipid molecule and not directly the surface density. As we have argued before, however, to first approximation these two quantities are proportional to each other, as an increase of water concentration has mainly the effect of “diluting” the bi-dimensional fluid formed by the molecular heads.

The nature of the structural changes associated to the different phase transitions has been mainly investigated in NMR experiments. NMR data [26] indicate that, starting from the ordered crystal phase, the transition to the gel phase corresponds to an order-disorder transition of the heads, in which the tails retain their order, but undergo a collective “tilt” with respect to the plane of the bilayer [25]. The transition to the liquid-crystal phase is related to a further order-disorder



transition, which this time involves also the tails.

The experiments that put in evidence the existence of these different phases are generally performed on liposomes (sort of artificial small cells) in solution or on the so-called Langmuir-Blodgett multi-layers and are commonly performed at constant pressure. In these conditions the surface density of phospho-lipid heads changes with temperature. On the simulation side the requirement of holding the pressure constant can be fulfilled by performing MD simulations in the (NpT) *ensemble*. Simulations of this type are rather delicate as they require sophisticated strategies to force the system to move in the phase space with the appropriate statistical weight and to tame otherwise annoying numerical instabilities. It should be immediately said, however, that today a lot of skill has been developed to properly deal with all these problems [2, 4, 6]. Simulations in the (NVE) (*micro-canonical ensemble*) are definitely much simpler and numerical stability is easily achieved. In the *micro-canonical ensemble* pressure and temperature are not independent variables and can in principle be determined once the values of the density, N/V , and total energy, E , are given.

Our strategy was to make a systematic study of the structural properties of the system by performing MD simulations at many different values of the (NVE) parameters in such a way as to explore quite a large set of values of temperatures and densities. The high “resolution” of our exploration has allowed us to draw interesting conclusions about the properties of the crystal and gel phase of the system. Results obtained for $BM(S)$ are confirmed by the analysis of the data we collected for the much larger system, $BM(L)$. As we shall see, $BM(L)$ data are affected by almost identical statistical errors as the $BM(S)$ data, though the available trajectories are much shorter.

3.1 Extracting physical information from simulations

Generally speaking, in order to show the existence of a phase transition one must be able to define an appropriate set of “order parameters” which could be used to describe the structure of the phase diagram of the system. The degree of order/disorder of the system can then be monitored through functions and parameters characterizing the translational and/or the orientational distribution functions of the constituent molecules. As a general reference for this kind of analysis, we shall follow in this paper the approach used in the discussion of liquid-crystal simulations in ref. [27].

As a first step in the study of the order properties of the system, we define the average direction of the constituent molecules. This quantity is represented by the 1-st rank order parameter

$$\vec{P}^{(\ell)} = \langle \langle \vec{u} \rangle \rangle^{(\ell)} \quad (1)$$

where, for elongate molecules, like the ones we are dealing with, the unit vector \vec{u} is naturally taken as the principal axis of the inertial tensor of the molecule (*i.e.* the normalized eigenvector of the inertial tensor with the lowest eigenvalue). The double bracket in eq. (1) means average over both the N_{mol} (identical) molecules of the system and over the N_{conf} configurations collected in the simulation. The superscript “ ℓ ” ($\ell=1,2$) means that the average is restricted to the ℓ -th layer (conventionally we decided to call layer #1 the upper layer and layer #2 the lower one). The z component of \vec{P} , which is usually called P_1 , will be used to monitor the average orientation of the molecules.

A further order parameter, which is also experimentally accessible (mainly in ^2H -NMR experiments [26]), that can be used to parametrize the local orientational order of molecular segments, is

$$S_i^{(\ell)} = \langle \langle \frac{1}{2}(3 \cos^2 \beta_i - 1) \rangle \rangle^{(\ell)} \quad (2)$$

where the superscript “ ℓ ” has the same meaning as in eq. (1). In NMR experiments β_i is the angle between the i -th carbon-deuterium ($\text{C}_i\text{-D}$) bond in a tail and the external static magnetic field (which is usually taken to coincide with the normal to the bilayer surface). S_i , often called “segmental order parameter”, defines a good order parameter as it enjoys the following characteristic properties

- When the $\text{C}_i\text{-D}$ bonds are essentially aligned in a given direction with respect to the magnetic field, the system is in an ordered phase with $S_i \simeq \frac{1}{2}(3 \cos^2 \beta^{(0)} - 1) \neq 0$, where $\beta^{(0)}$ is the most represented angular value in the distribution. In particular, if all the bonds have $\beta_i = 0$, then $S_i = 1$.
- When the distribution of $\cos \beta_i$ is flat (*i.e.* when all the values of $\cos \beta_i$ appear with equal probability), $S_i = 0$ and the system is in a completely disordered phase.

The crucial point that must be taken into account in trying to adapt the above definition to the situation one encounters in numerical simulations is that the order parameter we would like to define should allow us to distinguish in a clear way genuine order–disorder transitions from possibly present (and also very interesting) transitions between different kinds of ordered structures. The latter is precisely the situation that occurs experimentally in the $\text{crystal} \rightleftharpoons \text{gel}$ transition, where, as we recalled above, the phase transition appears to be characterized by the following two structural changes: 1) heads undergo an order–disorder transition, 2) tails remain ordered, but the angle made by their average direction with the normal to the plane of the bilayer increases significantly (tilt). The problem with the definition (2) is that, in the situation in which the reference axis is taken to be the

same for all tail segments and lie parallel to the bilayer normal, an overall change in the direction of the tails with respect to it will actually affect the value of the order parameter (making it smaller), much in the same way a real increase of the disorder of the tails would do.

To overcome this type of difficulties it was suggested in [27] that the way to appropriately monitor the local orientational order of atomic segments along the molecule is to use the formal expression given in eq. (2), but with β_i the Euler angles formed by the z axes of suitably chosen local reference frames (see below) with the average direction of the molecules in the layer to which the segments one is considering belong. Each local frame is defined by taking the z axis parallel to the segment connecting two non-contiguous carbon atoms along a tail.

Let us now see how these general considerations are translated into precise formulae. Since we are interested in investigating 2-nd rank tensor properties of the system, as those that are extracted from NMR experiments, it is convenient to measure order with respect to the directions of “maximum 2-nd rank order” [18, 28]. These directions are determined starting from the construction of the traceless tensor (whose definition closely parallels that of quadrupole moment of a charge distribution [29])

$$Q_{\alpha,\beta}^{(\ell)} = \langle \langle \frac{1}{2} (3 u_\alpha u_\beta - \delta_{\alpha\beta}) \rangle \rangle^{(\ell)} \quad \alpha, \beta = 1, 2, 3 \quad (3)$$

where \vec{u} is a unit vector related to the geometry of the molecules, δ is the Kronecker symbol and again one defines a Q -tensor for each one of the two layers. Eigenvalues and eigenvectors of Q reflect collective orientational properties of the system. For instance, if the phase is uniaxial (more mathematically, if the system is a collection of objects with $D_{\infty,h}$ point space group symmetry), \vec{u} should be taken as the direction of the principal axis of inertia of the molecules. Then Q will have one positive eigenvalue, say, λ (usually called P_2) and two identical negative eigenvalues, $-\lambda/2$. A biaxial phase is characterized by the fact that the two negative eigenvalues are not equal, while a more complicated orientational order is reflected in a non-trivial dependence of the eigenvectors of Q on the choice of \vec{u} . In the uniaxial phase the (normalized) eigenvector corresponding to the highest eigenvalue, λ , is called “director” and will be indicated by $\vec{d}^{(\ell)}$ in the following. In our case $\vec{d}^{(\ell)}$ represents the average direction of alignment of the long molecular axes in layer ℓ .

A precise notion of local order in each layer is introduced by comparing the orientation of a local rigid frame associated to any given molecular fragment with the orientation of a fixed reference frame, related to the collective order of the system, which we will identify with the (orthogonal) eigenvectors of $Q^{(\ell)}$. Given three non-aligned atoms, indexed by i_1 , i_2 and i_3 the local frame associated to

each fragment, i ($i \equiv i_1 i_2 i_3$), is constructed by taking the z axis as the vector joining the atom i_1 with the atom i_3 and the y - z plane as the plane where the three atoms lie. The azimuthal and polar angles (α_i and β_i) of the director $\vec{d}^{(\ell)}$ in these local frames can be used in turn to specify their orientation.

It is important to remark that, in comparing values of the order parameter, S_i , constructed through eq. (2) where the angles β_i are defined as described above, with numbers extracted from NMR experiments, the latter must be multiplied by a suitable numerical factor. This is related to the fact that in our definition of order parameter we monitor the orientation of the segment joining, say, the two non-contiguous C_i - C_{i+2} atoms, while the two experimentally relevant C_{i+1} -D bonds, whose average direction is extracted from NMR data, lie in a plane almost perpendicular to it. Given the relative orientation of the different reference systems we have introduced, it can be shown, using Wigner rotation matrices, that in our geometrical conditions this factor is always very near to -2 [26].

To monitor the translational order/disorder properties it is customary to make reference to the pair distribution function. Given the strong anisotropy of the molecule arrangement, typical of our system, it is convenient to define the two pair distribution functions, $g_{\parallel}(r_{\parallel})$ and $g_{\perp}(r_{\perp})$, where r_{\parallel} and r_{\perp} represent the length of the components of the vector joining the atoms of the pair in the direction parallel to the bilayer normal and in the plane perpendicular to it, respectively. As usual, g_{\parallel} and g_{\perp} are normalized to the corresponding ideal gas distributions at the same density. We thus write

$$g_{\parallel} = \frac{h_{\parallel}}{h_{\parallel}^g} \quad g_{\perp} = \frac{h_{\perp}}{h_{\perp}^g} \quad (4)$$

where $h(r)$ is the number of pairs of atoms at (parallel, or respectively perpendicular) distance equal to r and $h^g(r)$ is the corresponding quantity for the ideal gas at the same density. It should be noted that we separately define a g_{\perp} distribution for each one of the two layers by correspondingly limiting the calculation to the appropriate set of molecules.

3.2 Data analysis

For an ergodic system *micro-canonical* averages are computed as time averages of infinitely long trajectories. Such time averages are approximated in practice by averages over the largest possible number of independent configurations one can collect (given the available computing power) and representative of the infinite set of configurations of the system. As for the statistical error to be attributed to these *ensemble* averages, one should take the associated standard deviation.

A look at the time evolution of the $BM(S)$ system and, in particular, at the behaviour of the inter-molecular energy (E_{inter}) shows that a plateau is smoothly

reached in most cases only after about 2.5-3 ns. In view of this rather slow equilibration time we prudentially decided to exclude from the analysis presented in the next section the first 3 ns of each MD trajectory.

The situation is much better for the $BM(L)$ system for two reasons. One is that, as we explained before, the initial configuration of each $BM(L)$ simulation was obtained by replicating the (already well equilibrated) last available configuration of the $BM(S)$ system and further proceeding with an equilibration of the full system. The second is that the equilibration time of a larger system is naturally shorter.

To decide how distant in time two successive configurations should be in order to consider them as uncorrelated, we studied the auto-correlation function of the potential energy. In the case of the $BM(S)$ system, we found that, after removing from the analysis the configurations referring to the first 3 ns of each trajectory for the reasons explained above, the auto-correlation function dies away in a few ps at all values of density and temperature. A similar situation occurs in the case of the $BM(L)$ system (though all the available configurations, produced after the initial velocity-rescaling equilibration, were kept in the analysis). Accordingly, we then decided to record a configuration every 1000 long time-step iterations (*i.e.* every 5 ps) in all cases.

For the small system this means that we will have at our disposal not less than 480 uncorrelated configurations (and sometimes much more, up to 1380, see Table 1), that can be used in the forthcoming analysis. For the larger system $BM(L)$, where much shorter trajectories have been collected, averages will be taken over a significantly smaller number of configurations. Despite this fact, thanks to the much larger size of the sample $BM(L)$ compared to that of $BM(S)$, statistical errors turn out to be of comparable magnitude.

4 Results

Out of the many surface densities we have explored we will show data corresponding to the three cases, $\mu = 1.0$, 0.83 and 0.69, that roughly represent the experimental densities of the three most significant phases of the DMPC bilayer, *i.e.* crystal, gel and liquid-crystal, respectively. For each of these densities we will discuss results at three different temperatures (Tables 1 and 2). The temperatures we have considered were chosen so as to have them below, in between and above the two most significant phase transitions (crystal \rightleftharpoons gel and gel \rightleftharpoons liquid-crystal) the DMPC bilayer undergoes (see Fig. 2).

Despite the fact that we do not regard the results we obtained at the lowest density as physically interesting for the description of the expected liquid-crystal

i[!htbp]

Table 3: Inter-molecular (E_{inter}) and intra-molecular (E_{intra}) energies at some selected temperature-density points for the $BM(S)$ system. Numbers in the column labeled by T_s are the measured temperatures at which the corresponding simulation has actually run. Errors are in brackets.

T (K)	μ	T_s (K)	E_{inter} (kJ/mol)	E_{intra} (kJ/mol)
150	1.00	157 (2)	-207.5 (0.6)	84.8 (1.0)
150	0.83	151 (2)	-201.0 (0.6)	85.6 (0.9)
150	0.69	160 (2)	-195.9 (0.6)	96.5 (1.0)
275	1.00	283 (4)	-204.1 (1.0)	131.7 (1.6)
275	0.83	281 (3)	-196.7 (1.0)	132.3 (1.6)
275	0.69	294 (4)	-186.4 (1.0)	143.9 (1.6)
325	1.00	338 (4)	-199.7 (1.2)	154.6 (1.9)
325	0.83	341 (4)	-186.7 (1.2)	161.0 (1.9)
325	0.69	343 (5)	-185.0 (1.7)	175.8 (2.1)

phase of a bilayer, we will nevertheless briefly discuss them in this section, mainly to contrast these data with what we get at the more reliable values of the density, $\mu=1.0$ and $\mu=0.83$. This discussion may also be very useful to identify where and how our model should be improved.

4.1 The system $BM(S)$

We shall start our analysis by discussing the data we get from the simulations of the system $BM(S)$, for which we have collected very long trajectories (see Table 1). We will use the results coming from the $BM(L)$ system to refine and confirm the physical picture that emerges.

4.1.1 Thermodynamic properties

The density and temperature dependence of E_{inter} and P_2 should show marked variations in correspondence to first or second order phase transitions. In Table 3 a smooth and rather flat dependence of E_{inter} on T and μ is, instead, seen ³. This may be partly due to a still too coarse grid of points in the temperature and density plane and partly to the finite size of the simulated systems.

³In the third column of Table 3 we have reported the actual physical temperature, T_s , of each simulation.

Table 4: Values of the 1st rank order parameter, P_1 , at some selected temperature-density points, separately for the upper (#1) and the lower (#2) layer of the $BM(S)$ system. Errors are in brackets.

T (K)	μ	$P_1(\text{layer \#1})$	$P_1(\text{layer \#2})$
150	1.00	-0.909 (0.004)	0.891 (0.004)
150	0.83	-0.775 (0.003)	0.763 (0.004)
150	0.69	-0.637 (0.005)	0.627 (0.004)
275	1.00	-0.923 (0.005)	0.913 (0.005)
275	0.83	-0.788 (0.005)	0.782 (0.005)
275	0.69	-0.63 (0.02)	0.58 (0.02)
325	1.00	-0.914 (0.007)	0.924 (0.005)
325	0.83	-0.795 (0.007)	0.800 (0.007)
325	0.69	-0.46 (0.03)	0.73 (0.02)

At all values of density and temperature the molar heat capacity per atom, c_V , which was computed according to [30, 19], shows values in the range 3–3.5 (in units of the gas constant, R), which are typical of a molecular liquid.

As for the parameter P_1 (eq. (1)), we see from Table 4 that it is rather sensitive to the average orientation of the molecules with respect to the z -axis (which, we remember, coincides with the bilayer normal) and, as expected, it steadily decreases with the density.

Table 5: Same as in Table 4 for the 2nd rank order parameter, P_2 .

T (K)	μ	$P_2(\text{layer \#1})$	$P_2(\text{layer \#2})$
150	1.00	0.986 (0.002)	0.996 (0.001)
150	0.83	0.979 (0.004)	0.962 (0.003)
150	0.69	0.961 (0.004)	0.949 (0.005)
275	1.00	0.996 (0.001)	0.995 (0.001)
275	0.83	0.995 (0.001)	0.995 (0.001)
275	0.69	0.95 (0.02)	0.80 (0.02)
325	1.00	0.996 (0.001)	0.995 (0.001)
325	0.83	0.978 (0.008)	0.990 (0.002)
325	0.69	0.28 (0.05)	0.84 (0.02)

We remark that the values of the parameters P_1 , P_2 and d_z (see Tables 4, 5 and 6) for the two layers are consistent with each other within three (most often, two) standard deviations for the two highest values of μ (*i.e.* $\mu=1.0$ and

0.83). There is instead a statistically significant difference, especially at the highest temperatures, if one compares values referring to the upper and lower layer at the lowest density. This is due to rare events in which some of the molecules in the upper/lower layer rotate upward/downward relatively to the bilayer plane. Unfortunately the characteristic times of these motions are too long compared to the length of the trajectories we have produced to be in position of adequately sampling this dynamics. It is then not surprising to find that, within the time window of our simulations, the two layers do not appear statistically identical.

Table 6: Same as in Table 4 for the director z component, d_z .

T (K)	μ	d_z (layer #1)	d_z (layer #2)
150	1.00	0.913 (0.004)	0.892 (0.004)
150	0.83	0.781 (0.003)	0.773 (0.004)
150	0.69	0.646 (0.005)	0.639 (0.004)
275	1.00	0.924 (0.005)	0.914 (0.005)
275	0.83	0.790 (0.005)	0.783 (0.005)
275	0.69	0.67 (0.02)	0.1 (0.7)
325	1.00	0.915 (0.007)	0.926 (0.006)
325	0.83	0.801 (0.007)	0.803 (0.007)
325	0.69	0.6 (0.2)	0.83 (0.01)

Although we do not see any sign of instability of our bilayer model at anyone of the values of density and temperature we have explored (we have performed simulations at densities as low as $\mu=0.69$ and temperatures as high as $T=350$ K) or after very long simulation times (some of the trajectories are as long as ~ 10 ns), we will not consider data referring to $\mu=0.69$ as physically significant, in view of the undesired behaviour described above.

All the data presented in this section are consistent with the description of the bilayer as an oriented molecular liquid, if one excludes the density $\mu=0.69$, where the system starts to show an increasing degree of isotropy. As for other structural parameters, particularly the pair distribution functions (see below), they show a high level of translational order that is progressively lost when the density decreases or the temperature increases. Finally, it is worth noticing that decreasing the density affects the orientational order in a stronger way than increasing the temperature, indirectly suggesting that ordering is more sensitive to hydration than to heating.

4.1.2 Structural properties

We start by discussing some general structural properties of the bilayer at selected density-temperature points, that are suggested by a simple graphical inspection of the geometry of the system. In Figs. 3 and 4 we show two views ((a) and (b)) of two snapshots of the larger bilayer, $BM(L)$, at $T=325$ K and at the two densities, $\mu=1$ and 0.83 , respectively. The snapshots are obtained using the program MOLMOL [31]. In panel (a) of Figs. 3 and 4 we show the side view of the bilayer as seen from the direction in the x - y plane from which the translational order of the upper layer is most clearly visible. In panel (b) of Figs. 3 and 4 we show the top view of the same pictures, obtained after rotating the bilayer by 90° around an axis orthogonal to both the z axis and the direction of “best view” identified above. As a whole, the figures show that the main effect of decreasing the density is a progressive tilt in the average orientation of the molecules with respect to the bilayer normal.

Further information on the translational order properties of the system can be gained by looking at Figs. 5 and 6, where we have plotted at the two (density, temperature) values considered above, namely (a)=(1, 325 K) and (b)=(0.83, 325 K), the projections on the x - y plane of the segment joining the two atoms of the pair C10-C13 (Fig. 5) and C24-C37 (Fig. 6), as they evolve in time. The two pairs we consider are taken to belong to the upper layer. They differ in their average distance from the middle plane lying in between the two layers: the C10-C13 pair can be used to describe the orientation of the head, as the two atoms belong to the top portion of the lipid molecule, while the C24-C37 pair can be used to monitor the orientation of the imaginary rectangle roughly containing the two molecular tails, because the C24 and C37 atoms belong to different tails and are located at more or less the same height from the C13 joint. A remarkable feature, quite evident in all the figures, is that molecules undergo fluctuations in local positional energy minima that are spatially well ordered at high density and progressively less ordered as the density decreases. An other interesting question that can be studied by analyzing Figs. 5 and 6 is the effect of density on the degree of molecule packing: the range of positional fluctuations at $\mu=0.83$ is smaller than that at the higher density, $\mu=1$, both for heads (Fig. 5) and tails (Fig. 6). This means that the larger space the molecules have at their disposal, going from higher to lower densities, does not directly influence their actual translational freedom. The reason for this behaviour may be due to the fact that a decrease of the interaction potential among the molecules in each layer (that occurs because molecules are more separated) is at least partly compensated by the stronger interaction potential between the two layers (which follows from the fact that an increase of the molecular tilt angle decreases the distance between the two layers).

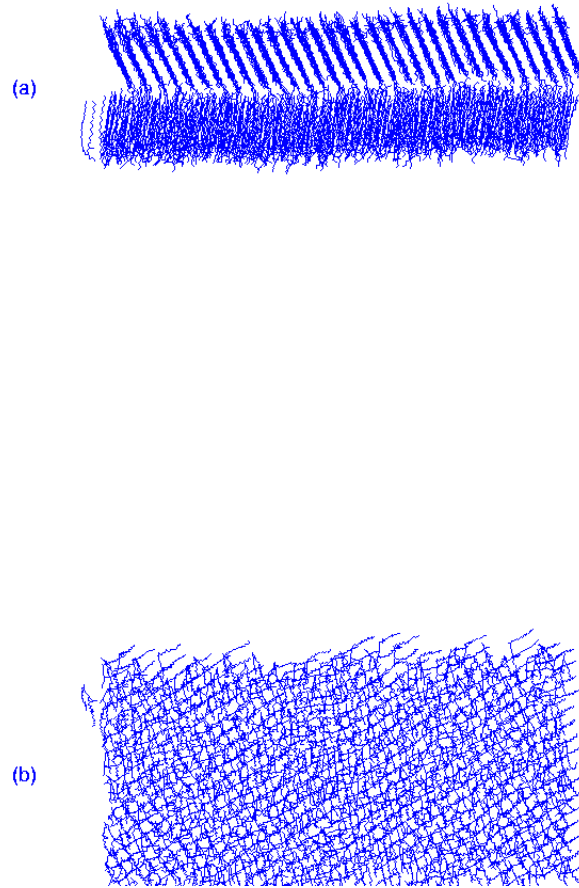


Figure 3: The final configuration of the $BM(L)$ simulation at $\mu=1$ and $T=325$ K: side view (a), top view (b).

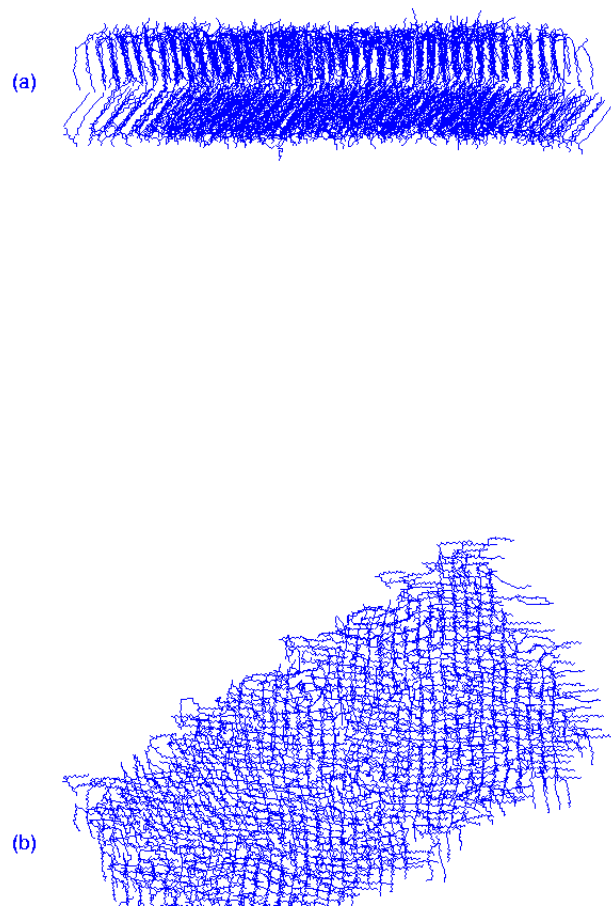


Figure 4: Same as in Fig. 3 at $\mu=0.83$ and $T=325$ K.

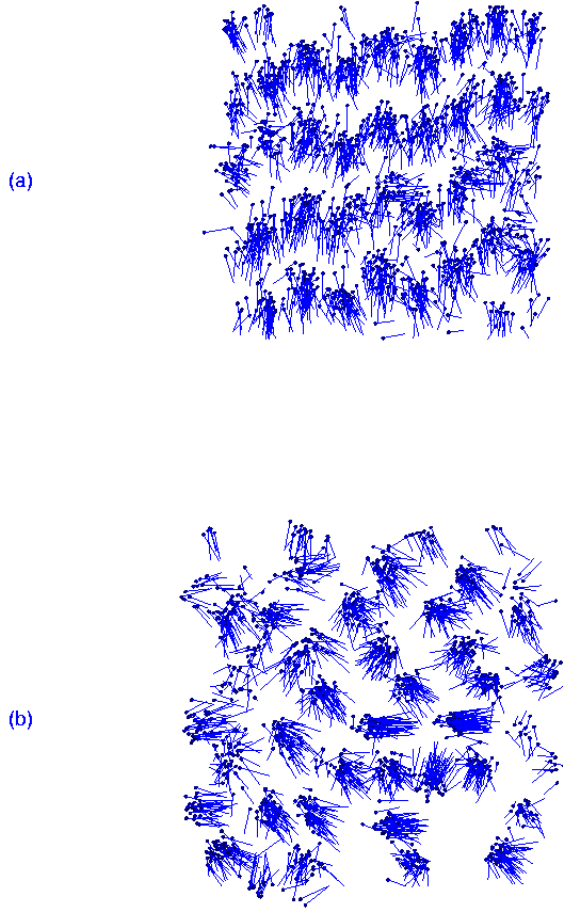


Figure 5: The projections on the x - y plane of the vectors joining the pair of atoms C10-C13, as seen in selected configurations of the $BM(S)$ trajectory at $T=325$ K and $\mu=1$ (a), $\mu=0.83$ (b).

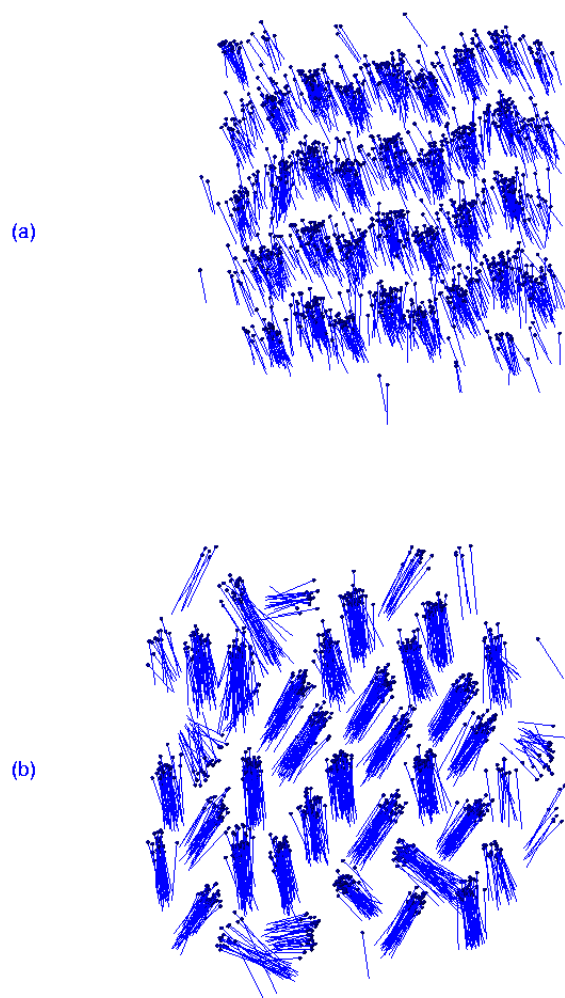


Figure 6: Same as in Fig. 5 for the C24-C37 pair of atoms.

Finally, an inspection to the geometry of single molecules in different density-temperature conditions shows that at $\mu=1$, $T=150$ K, the longer C15-C46 tail (tail #2) lies essentially parallel to the head, while the O14-C31 tail (tail #1) shows a kink in correspondence to the dihedral angle O14-C17-C19-C20, making it parallel to tail #2 after C19. This geometric arrangement, that is present in the initial crystallographic structure [16], becomes “inverted” at smaller densities and even at $\mu=1$ at the highest temperature, $T=325$ K, in the sense that the kink appears instead in the longer tail #2. In this situation the two tails happen to have almost the same effective length, if counted from the common branching point, C13. The related torsional changes occurring in the neighborhood of the branching region seems to be a very important ingredient in arranging the internal molecular structure so as to comply with the tilting and packing of molecules taking place in each layer.

4.1.3 Pair distribution functions

The information obtained through the graphical investigations we have just described can be quantified in a useful way with the help of the pair distribution functions and the order parameters defined in the previous section.

In Fig. 7 the g_{\perp} distribution of C10 (panel (a)) and C24 pairs (panel (b)) at $T=325$ K and for the three densities, $\mu=1$, 0.83 and 0.69, are compared. C10 is the group that replaces the charged part of the head of the DMPC molecule in our DMMG model, while C24 is a group located in the deep hydrophobic region. We see a significant difference in the translational structure between heads and tails, which is present at all densities: tails (panel (b)) look definitely more ordered than heads (panel (a)). At $\mu=1$ both tails and heads are ordered (see Fig. 8 and the solid line in Fig. 7 (b)): the system appears to be in a crystal phase. Of course ordering of the heads is progressively lost by increasing the temperature, as seen by comparing Fig. 7 (a) with Fig. 8. At $\mu=0.83$ tails are still ordered but heads shows a structure which looks more liquid-like. This is very much indicative of a gel phase. Finally at the lowest density, $\mu=0.69$, we see a strong disordering of the tails, owing to molecular upward/downward rotation, with a consequent tendency to isotropization. Looking at the shape of the dotted curve in Fig. 7 (b) and at the P_1 and P_2 data at $\mu=0.69$ in Tables 4 and 5, we are thus led to the conclusion that at this density the system finds itself in a configuration which is much too isotropic to be possibly interpreted as the liquid-crystal phase of a bilayer. It should be noticed, however, that tail disordering does not seem to affect the value of the inter-molecular energy, because, as we noticed above, the potential energy loss in each layer is compensated by a stronger interaction energy between the two layers.

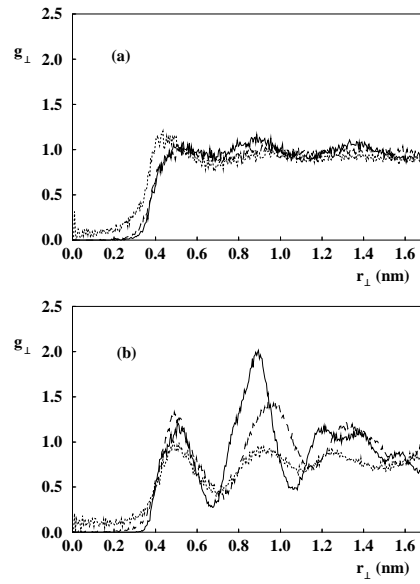


Figure 7: The g_{\perp} pair distribution function of C10 (a) and C24 (b) atoms for the system $BM(S)$ at $T=325$ K and $\mu=1$ (solid line), $\mu=0.83$ (dashed line), $\mu=0.69$ (dotted line).

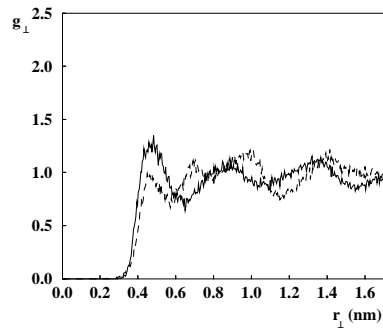


Figure 8: The g_{\perp} pair distribution function of C10 atoms for the system $BM(S)$ at $T=150$ K and $\mu=1$ (solid line), $\mu=0.83$ (dashed line).

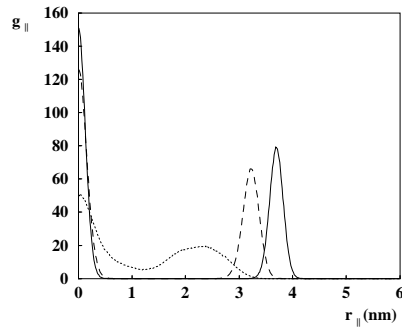


Figure 9: The g_{\parallel} pair distribution function of C13 atoms for the system $BM(S)$ at $T=325$ K and $\mu=1$ (solid line), $\mu=0.83$ (dashed line), $\mu=0.69$ (dotted line).

There is a correlation among the decrease in density, the tilt of the molecules in the two layers and the decrease in the bilayer thickness. In Fig. 9 we plot the g_{\parallel} pair distribution functions of C13 atoms, again for $T=325$ K at the three decreasing densities, $\mu=1$ (solid line), 0.83 (dashed line) and 0.69 (dotted line). The first thing that should be noted is the presence of very pronounced peaks at $r_{\parallel} \approx 0$. These peaks come from the contributions of pairs of atoms belonging to the same layer. Concentrating our attention to the region $r_{\parallel} > 0.5$ nm, we see that the solid and dashed curves show narrow peaks, sticking out over a region of vanishing g_{\parallel} , centered at $r_{\parallel} \approx 3.8$ nm and $r_{\parallel} \approx 3.3$ nm, respectively. They are indicative for the existence of two well separated layers. We remark that the first number is not too far from the value of the experimental bilayer thickness, which is ≈ 4 nm at the same density and temperature. The shift in the location of this peak is nicely explained by the progressive molecule tail tilting, taking place by lowering the density, which tends to reduce the bilayer thickness. The overall shape of the dotted curve in Fig. 9 is, instead, completely different: first of all the rightmost peak is much broader than the corresponding peak seen in the other two curves and secondly there is no region where g_{\parallel} is zero: in fact, pretty soon, to the left of the rightmost peak g_{\parallel} starts to grow again. This behaviour reflects the fact that at this density the two layers partially overlap, as a consequence of the tendency to isotropization described above. Again, we notice that the effect of increasing the temperature on the bilayer thickness is negligible, if compared to what happens when we lower the density. For instance, increasing the temperature from 150 K to 325 K produces a thickness variation (which is maximal at $\mu=0.83$) of only 0.3 nm, while by decreasing the density from $\mu = 1$ to $\mu = 0.83$ and from $\mu = 0.83$ to $\mu = 0.69$, the peak in Fig. 9 gets shifted by ≈ 0.5 nm and ≈ 1 nm, respectively.

4.1.4 Angular Distributions

In Fig. 10 we show the distribution function $P(\theta)$ of the polar angle, θ , formed by the bilayer normal with the z axis of the local frame identified by the atoms C34-C40-C46 of tail #2. This direction, which, we recall, is chosen to be parallel to the vector joining the C34-C46 atoms, is practically aligned with the long molecular axis. We show the results for the lower layer only, as data for the other layer are essentially identical. The progressive tail tilting of the molecules with decreasing density is clearly visible. We also see that the peak of the distribution moves from 25° at $\mu=1$ (long-dashed line) to 40° at $\mu=0.83$ (short-dashed line). At the lowest density (dotted line) the distribution becomes rather broad, but still peaked around 40° . The experimental tilt angle for similar systems in the gel phase, which has been measured to be about 30° [32], is well consistent with these results. We

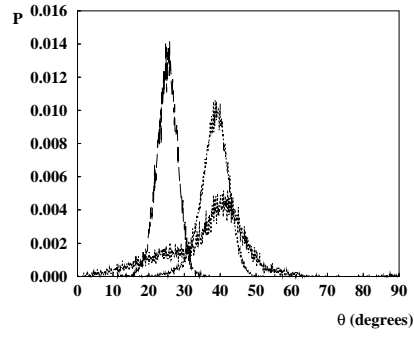


Figure 10: The distribution function at $T=325$ K of the angle, θ , formed by the segment C34-C46 of tail #2 with respect to the bilayer normal, for the $BM(S)$ system at $\mu=1$ (long-dashed line), $\mu=0.83$ (short-dashed line) and $\mu=0.69$ (dotted line).

regard this agreement as a success of our model.

A final structural investigation has been performed on the population of the different torsional states along the tails. Since the local torsional potential has three energy wells, corresponding to two *gauche* states ($\phi=60^\circ$ and 300°) with the same energy and one *trans* state ($\phi=180^\circ$) with a different energy ⁴, we can adequately characterize the situation by a parameter, usually called P_g , which represents the percentage of the total *gauche* population belonging to each torsion. We find at $T=325$ K the results reported in Table 7. In this computation we have averaged data over the two tails and the two layers. Values smaller than 1 % are not reported.

Table 7: Percentage (%) of population of tail torsions at $T=325$ K for the $BM(S)$ system at the various densities. Values smaller than 1% are not reported.

<i>Torsion</i>	$\mu=1$	$\mu=0.83$	$\mu=0.69$
(C12-C13-O14-C17)+(C13-C15-O16-C32)	23	25	24
(C13-O14-C17-C19)+(C15-O16-C32-C34)	4	4	7
(O14-C17-C19-C20)+(O16-C32-C34-C35)	50	50	44
(C17-C19-C20-C21)+(C32-C34-C35-C36)	1	10	7
(C19-C20-C21-C22)+(C34-C35-C36-C37)	-	2	6
(C20-C21-C22-C23)+(C35-C36-C37-C38)	-	2	5
(C21-C22-C23-C24)+(C36-C37-C38-C39)	-	1	5
(C22-C23-C24-C25)+(C37-C38-C39-C40)	-	1	5
(C23-C24-C25-C26)+(C38-C39-C40-C41)	-	1	4
(C24-C25-C26-C27)+(C39-C40-C41-C42)	-	1	5
(C25-C26-C27-C28)+(C40-C41-C42-C43)	-	1	5
(C26-C27-C28-C29)+(C41-C42-C43-C44)	-	1	6
(C27-C28-C29-C30)+(C42-C43-C44-C45)	1	4	8
(C28-C29-C30-C31)+(C43-C44-C45-C46)	3	6	9

At the two highest densities only the last two torsions (C27-C28-C29-C30, C28-C29-C30-C31) in tail #1 and the corresponding ones in tail #2 show a population larger than 1%. The high values, $P_g=25\%$ and $P_g=50\%$, that we find for the average percentage population in the torsions (C12-C13-O14-C17) + (C13-C15-

⁴Actually the energy of the *trans* state is lower than the energy in the *gauche* states in all torsions involving only aliphatic carbons.

O16-C32) and (O14-C17-C19-C20) + (O16-C32-C34-C35), respectively, are due to the distortion of the geometry in the “kinked” region close to the ester bond. These values are essentially the same for all densities and temperatures and are due to the phenomenon of “kink inversion” between the two tails, described before. It is worth noticing that the $\mu=0.83$ results are consistent with those obtained for the DPPC in the gel phase [2, 4], after correcting for the fact that the DPPC hydrophobic tails are 2 methylene groups longer than the DMPC tails.

The smooth increase of the *gauche* population along the tails, seen in the simulations performed at the lowest density, means that the rotational freedom of molecule tails does not help in making the tail flexibility in the terminal region larger than that in the core. This is at variance with the results of the first paper of ref. [4], where a larger mobility of tail end segments, as compared to what is seen in the core region, was found in simulations of the liquid-crystal phase of DPPC. Values around 20 % for P_g for the last six torsions of the tails are, in fact, reported. One might argue that the little tail flexibility we find in our model might be attributed to the much too strong 1-4 LJ potential we have introduced in each torsion. These 1-4 forces mainly have the effect of adding a steric repulsion in the *gauche* conformations. We recall that within the framework of the OPLS force-field [20], which we employed in the present paper, we have reduced, according to the general OPLS philosophy, the strength of the 1-4 LJ potential by a factor 8. This may not have been enough in view of the too high tail rigidity we have found. However, neglecting 1-4 forces altogether gives results only partially in the desired direction. In fact, on the one hand it actually produces an increase of the *gauche* population by a large factor (in trial simulations performed on liquid butane this factor is found to be about 3), but on the other hand it leads to a more pronounced upward/downward molecular rotational freedom, which may make even more problematic for the system to unveil its liquid-crystal phase.

4.1.5 Segmental Order Parameter

In Fig. 11 we show the behaviour of the order parameter, S_i (eq. (2) of sect. 3.1), as function of the position of the (C_i-C_{i+2}) segment along the tail ⁵. Panels (a) and (b) show the results for tail #1 and #2, respectively, averaged over the two layers. We focus on the behaviour of S_i at $T=325$ K and different densities. We see that, correctly, the order parameter decreases with the density (the expectation for a completely isotropic fluid would be $S_i=0$). Notice that, not surprisingly, data at the lowest density are affected by errors that are definitely larger than those on

⁵We observe that the notation (C_i-C_{i+2}) does not apply to the initial segments of the two tails, that are called C17-C20 and C32-C35 respectively, because in the enumeration of carbons the labels 18 and 33 are attributed to O atoms.

the data at $\mu=1$ and $\mu=0.83$.

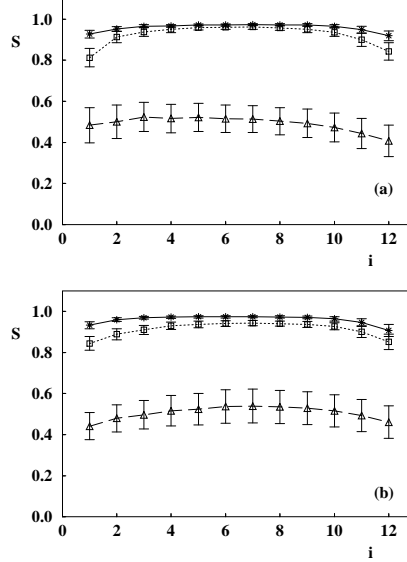


Figure 11: The S order parameter for the system $BM(S)$ at $T=325$ K as a function of the position along tail #1 (a) and tail #2 (b): stars are for $\mu=1$, squares for $\mu=0.83$ and triangles for $\mu=0.69$. The first segment starts from the carbonyl carbon atom C17 in tail #1 and C32 in tail #2. The lines joining the points are only to guide the eye.

4.2 The system $BM(L)$

As summarized in Table 2, we have performed extensive MD simulations also on the much larger system, $BM(L)$, consisting of 2 layers of 256 DMMG molecules each. To compare with previous results we have analyzed the trajectories corresponding to the same combined values of surface density and temperature considered above. An immediate observation that emerges from the analysis of $BM(L)$ MD data is that statistical errors are about the same as those one finds in the case of the system $BM(S)$, despite the fact that substantially shorter trajectories were produced (compare Tables 1 and 2). As we already noticed, this is a direct consequence of the increase in the size of the system and of the fact that the larger $BM(L)$ system was built by assembling already equilibrated $BM(S)$ blocks with the result that

no special needs for further long or sophisticated equilibration procedures have emerged.

The general conclusions of the analysis of $BM(L)$ data is that the scenario we have come up with in the previous sections is well confirmed by the simulations of this larger system, and we have good consistency between the two sets of data within errors.

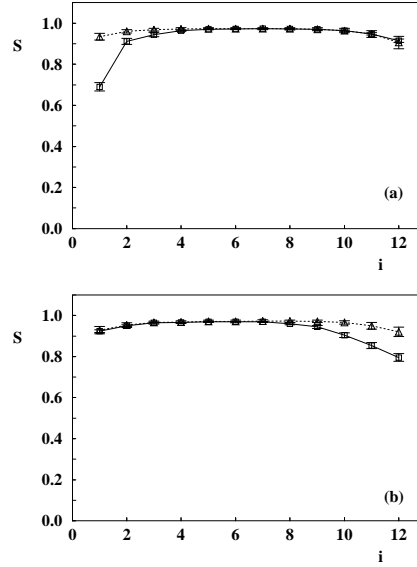


Figure 12: The S order parameters at $T=325$ K and $\mu=1$ as function of the position along tail #1 (a) and tail #2 (b) for the $BM(L)$ system (squares) and for the $BM(S)$ system (triangles). The lines joining the points are only to guide the eye.

As an example of the quality of the results that we have obtained, we compare in Figs. 12 and 13 the behaviour of the order parameter S , for the two systems, $BM(S)$ and $BM(L)$ at $T=325$ K and $\mu=1$ and $\mu=0.83$, separately for the two tails, averaged over the two layers. The $BM(L)$ points are systematically lower than the $BM(S)$ data, as expected from the lowering of the collective orientational order with the increasing size of the system. This effect is more relevant for segments close to the head and to the end of the tails. The slightly larger errors that affect the data associated to the first and the last tail segment are due to jumps among different torsional states that are not sufficiently well sampled in the time evolution at our disposal. In order to reduce errors associated to this

slow torsional dynamics, it would be important to increase the length of $BM(L)$ simulations. Data at $\mu=0.69$ are affected by substantially larger errors and are not shown.

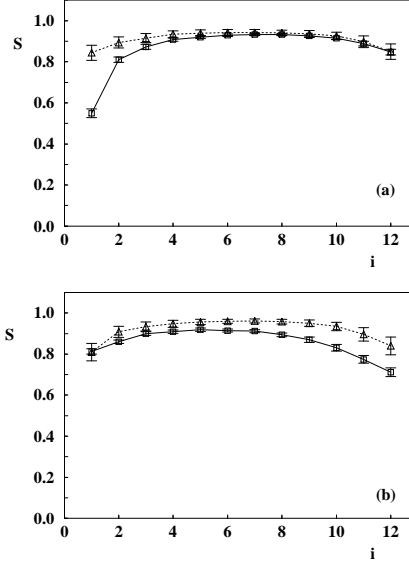


Figure 13: Same as in Fig. 12 at $\mu=0.83$.

The above indications about the behaviour of the degree of collective orientational order with the size of the system are confirmed by a careful study of the order parameters, P_1 and P_2 . For instance, at $\mu=0.83$ and $T=325$ K one gets for the $BM(L)$ system $P_2=0.964 \pm 0.003$, a value somewhat lower than the one observed for the smaller $BM(S)$ system, for which an average value $P_2=0.984 \pm 0.002$ is found. A lowering of the orientational order with the size of the system is actually expected from the observation that in a bigger system fluctuations with longer wave lengths are possible.

Further agreement among $BM(L)$ and $BM(S)$ simulations emerges from the study of translational order properties. The $g_{\perp}(r)$ distribution functions computed from the $BM(L)$ simulations show essentially the same structure and locations of the peaks that is seen in the $BM(S)$ distributions. The only difference is a somewhat less pronounced peak structure in distributions referring to atoms belonging to the hydrophobic core. Given the strong similarity of $BM(L)$ and $BM(S)$ results, we do not report the former here.

We would like to conclude this section with some general considerations about

the quest for MD simulations of larger and larger systems. Given the satisfactory level of consistency we find by comparing the MD data of the two samples, one might ask whether simulations of systems as large as $BM(L)$ are really necessary to get the physics of the system right. Although the answer to this question strongly depends on the kind and the degree of detail of the information one wishes to obtain from the model, it is important to recall that the study of finite volume effects is a necessary step in any numerical simulation, because features and properties seen at small volumes may completely change when the volume is increased. Consequently it is absolutely mandatory to get an idea of the magnitude of finite volume corrections. From our experience it was only thanks to the data we had for the larger system that we could reliably draw useful conclusions on the structural properties of our model-membrane.

Apart from these rather general considerations, there are in our opinion many specific problems where the fact of having a sufficiently large system is crucial in order to be in the position of extracting reliable results from numerical simulations. Just to make two examples we may mention:

1) the problem of trying to accurately locate the critical lines of the phase diagram of the system. The obvious reason for the necessity of comparing systems of different sizes is that a structural change of the system can be interpreted as a true phase transition only if one is able to show that the transition becomes sharper and sharper as the volume increases.

2) Another very interesting problem is the study of the dynamic and the formation of ion channels. In this case dealing with a sufficiently large system is required by the need of having the cross section of the channel sufficiently smaller than the surface of the bilayer itself in order to meet as accurately as possible the actual physical situation. We wish to mention in this context the pioneering investigation recently carried out in the beautiful work of ref. [7], where it has been shown that indeed channels have the possibility of forming and dynamically maintaining themselves stable.

5 Conclusions

We have performed a systematic MD study of the structural properties of a simple atomistic model of bilayer by analyzing the behaviour of a large number of physical quantities characterizing the system, as functions of density and temperature, and by comparing results obtained from simulations carried out on two systems of largely different size.

We have found that our modelization reproduces in a remarkable way many known features of the gel phase of DMPC bilayers [25], as well as the structural

changes that accompany the transition from the crystal to the gel phase. These findings have emerged quite clearly by analyzing the very long trajectories we have collected for the system, $BM(S)$, and are nicely confirmed by the statistically equally accurate data we have for the much larger system, $BM(L)$.

Clearly a lot of work is still needed to further validate and improve our approach, especially in the direction of investigating the role of water, whose effects were only indirectly accounted for through the modulation of the surface density of the system. The inability of the model to cope with the expected liquid-crystal phase of the system at low density is its major limitation. To prevent the extrusion of the molecule tails from the planes of the bilayer at low density and high temperature, either some sort of geometric or dynamic constraint must be introduced, perhaps by modifying the intra-molecular tail flexibility, or more directly one should explicitly introduce water.

Despite the limitations we have mentioned, from the quality of the results presented in this investigation, we conclude that the membrane model we have developed is capable of capturing most of the essential structural properties of the real system in the crystal and gel phase. Thanks to its simplicity, we are confident that it will be possible to appropriately improve the model in the directions mentioned above, without affecting the key features that are at the basis of the stability of our bilayer, *i.e.* tail packing within the layers and adequately strong interactions between the two layers.

Acknowledgments - We wish to thank G. Ciccotti and S. Melchionna for discussions. We also thank the ENEA Computing Center (Casaccia - Italy) and CINECA (Bologna - Italy), where most of the computations presented here have been performed and the APE groups of the Universities of Rome *La Sapienza* and *Tor Vergata* for their assistance. Partial support from the Italian Institutions INFN, INFM, CNR and MURST is gratefully acknowledged.

References

- [1] H. Heller, M. Schaefer and K. Schulten, J. Chem. Phys. **97** (1993) 8343.
- [2] D.J. Tobias, K. Tu and M.L. Klein, in Proceedings of the Como Conference *Monte Carlo and Molecular Dynamics of Condensed Matter Systems*. Eds. K. Binder and G. Ciccotti (Editrice Compositori, Bologna 1996), 325.
- [3] K. Tu, D.J. Tobias and M.L. Klein, J. Phys. Chem. **99** (1995) 10035.
- [4] K. Tu, D.J. Tobias and M.L. Klein, Biophys. J. **69** (1995) 2558;
K. Tu, D.J. Tobias, J.K. Blasie and M.L. Klein, Biophys. J. **70** (1996) 595;

- T. Husslein, D.M. Newns, P.C. Pattnaik, Q. Zhong, P.B. Moore and M.L. Klein, J. Chem. Phys. **109** (1998) 2826.
- [5] H.J.C. Berendsen, invited talk at the Symposium on *Multi-scale phenomena and their simulation*, Bielefeld, 1996. Eds. F. Karsch, B. Monien and H. Satz (World Scientific, Singapore 1997).
- [6] I.Z. Zubrzycki, Y. Xu, M. Madrid and P. Tang, J. Chem. Phys. **112** (2000) 3437.
- [7] G.R. Dieckmann, J.D. Lear, Q. Zhong, M.L. Klein, W.F. DeGrado and K.A. Sharp, Biophys. J. **76** (1999) 618.
- [8] R.M. Venable, B.R. Brooks and R.W. Pastor, J. Chem. Phys. **112** (2000) 4822.
- [9] R. Goetz and R. Lipowsky, J. Chem. Phys. **108** (1998) 7397;
R. Goetz, G. Gompper and R. Lipowsky, Phys. Rev. Lett. **82** (1999) 22.
- [10] R.W. Pastor, R.M. Venable and M. Karplus, Proc. Natl. Acad. Sci. USA **88** (1991) 892.
- [11] J.G. Gay and B.J. Berne, J. Chem. Phys. **74** (1981) 3316.
- [12] H. Zewdie, J. Chem. Phys. **108** (1998) 2117.
- [13] M.A. Bates and G.R. Luckhurst, J. Chem. Phys. **110** (1999) 7087.
- [14] R. Lipowsky and E. Sackmann, eds., *Structure and Dynamics of Membrane*, Handbook of Biological Physics (North Holland, Amsterdam 1995).
- [15] M.S. Markov, “*Role of water in forming and stabilizing membrane structure*”, in *Water and ions in biological systems*. Eds. P. Läuger, L. Packer and V. Vasilescu (Birkhäuser, 1988).
- [16] R.H. Pearson and I. Pascher, Nature **281** (1979) 499;
H. Hauser, I. Pascher, R.H. Pearson and S. Sundell, Biochimica and Biophysica Acta **650** (1981) 21.
- [17] R. Car and M. Parrinello, Phys. Rev. Lett. **55** (1985) 2471.
- [18] M.P. Allen and D.J. Tildesley, *Computer Simulation of Liquids* (Clarendon Press, Oxford 1990).
- [19] G. La Penna, V. Minicozzi, S. Morante, G.C. Rossi and G. Salina, Comp. Phys. Comm. **106** (1997) 53.

- [20] W.L. Jorgensen, J.D. Madura and C.J. Swenson, J. Am. Chem. Soc. **106** (1984) 6638;
W.L. Jorgensen, J. Phys. Chem. **90** (1986) 1276;
W.L. Jorgensen and J. Tirado-Rives, J. Am. Chem. Soc. **110** (1988) 3469.
- [21] N.A. Wilson and A. Pohorille, J. Am. Chem. Soc. **116** (1994) 1490.
- [22] M. Tuckerman, G.J. Martyna and B.J. Berne, J. Chem. Phys. **97** (1992) 1990;
D.D. Humphreys, R.A. Friesner and B.J. Berne, J. Phys. Chem. **98** (1994) 6885;
M. Watanabe and M. Karplus, J. Chem. Phys. **99** (1993) 8063; J. Phys. Chem. **99** (1995) 5680.
- [23] P. Procacci and B.J. Berne, J. Chem. Phys. **101** (1994) 2421.
- [24] The Ape Collaboration, Int. J. High Speed Comput. **5** (1993) 637.
- [25] M. Janiak et al., J. Biol. Chem. **254** (1979) 6068;
G.S. Smith, E.B. Sirota, C.R. Safinya and N.A. Clark, Phys. Rev. Lett. **60** (1988) 813.
- [26] J.-P. Douliez, A. Léonard and E.J. Dufourc, Biophys. J. **68** (1995) 1728.
- [27] G. La Penna, D. Catalano and C.A. Veracini, J. Chem. Phys. **105** (1996) 7097.
- [28] C. Zannoni, in *Molecular Physics of liquid crystals*, Eds. G.R. Luckhurst and G.W. Gray (Academic Press, London 1973), Ch. 9, 191.
- [29] C.P. Slichter, *Principles of Magnetic Resonance*, Springer Series in Solid-State Science 1 (Springer, Berlin 1996).
- [30] J.L. Lebowitz, J.K. Percus and L. Verlet, Phys. Rev. **153** (1967) 250.
- [31] R. Koradi, M. Billeter and K. Wütrich, J. Mol. Graphics **14** (1996) 51.
- [32] S. Tristram-Nagle, S.R. Zhang, R.M. Suter, C.R. Worthington, W.-J. Sun and J.F. Nagle, Biophys. J. **64** (1993) 1097.